Dynamic modeling of the heat pipe-assisted annealing line

Celik, Metin; Patki, Mrunal; Paulussen, Geert; De Jong, Wiebren; Boersma, Bendiks Jan

DOI
10.1115/1.4042701

Publication date
2019

Document Version
Final published version

Published in
Journal of Heat Transfer

Metin Celik[1]
Faculty of Mechanical,
Maritime and Materials Engineering,
Process & Energy Department,
Delft University of Technology,
Leeghwaterstraat 39,
Delft 2628 CB, The Netherlands
e-mail: M.Celik@tudelft.nl

Mrunal Patki
Process & Energy Department,
Faculty of Mechanical,
Maritime and Materials Engineering,
Delft University of Technology,
Leeghwaterstraat 39,
Delft 2628 CB, The Netherlands
e-mail: Mpatki0705@gmail.com

Geert Paulussen
Research & Development,
Tata Steel,
P.O. Box 10000,
Ijmuiden 1970 CA, The Netherlands
e-mail: geert.paulussen@tatasteeleurope.com

Wiebren de Jong
Process & Energy Department,
Faculty of Mechanical,
Maritime and Materials Engineering,
Delft University of Technology,
Leeghwaterstraat 39,
Delft 2628 CB, The Netherlands
e-mail: Wiebren.deJong@tudelft.nl

Bendiks Jan Boersma
Process & Energy Department,
Faculty of Mechanical,
Maritime and Materials Engineering,
Delft University of Technology,
Leeghwaterstraat 39,
Delft 2628 CB, The Netherlands
e-mail: B.J.Boersma@tudelft.nl

Dynamic Modeling of the Heat Pipe-Assisted Annealing Line

In a conventional continuous annealing line, the energy supplied to steel strip during heating is not recovered while cooling it. Therefore, an alternative heat transfer technology for energy efficient continuous annealing of steel was developed. This technology enables reusing the heat extracted during cooling of the strip in the heating part of the process. This is achieved by thermally linking the cooling strip to the heating strip via multiple rotating heat pipes. In this context, the dynamic simulation of a full heat pipe assisted annealing line is performed. The dynamic simulation consists of the interaction of computational building blocks, each comprising of a rotating heat pipe and strip parts wrapped around the heat pipe. The simulations are run for different installation configurations and operational settings, with the heat pipe number varying between 50 and 100 and with varying strip line speed and dimensions. The heat pipes are sized to be 0.5 m in diameter and 3 m in length. The simulation results show that the equipment is capable of satisfying the thermal cycle requirements of annealing both at steady-state and during transition between steady-states following changes in boundary conditions. With this concept, energy savings of up to 70% are feasible. [DOI: 10.1115/1.4042701]

1 Introduction

The cold rolling of steel results in the increase of the material's hardness due to dislocations induced by this process. In order to reduce its hardness and to render it more workable, steel is thermally treated by heating it to approximately 700 °C and then cooling it down to room temperature. This process is called annealing and it is an energy intensive process [1]. The current state of the art is to heat the steel strip using natural gas fired furnaces and to cool it down with a convective gas cooling system. In a conventional annealing line, the energy supplied to steel during heating is not recovered. Moreover, none of the energy is retained in the final product.

Therefore, an alternative technology for energy efficient annealing of steel was developed. This novel concept, called "heat pipe assisted annealing," aims to reduce the energy consumption to 30% of a conventional line [2]. The technology is based on multiple rotating heat pipes, thermally linking the heating strip to the cooling strip (Fig. 1).

A rotating heat pipe is a cylindrical two-phase heat transfer device rotating around its axis. It contains a fixed amount of working fluid, fully sealed inside. It is composed of three sections, namely the evaporator section, the adiabatic section, and the condenser section [3]. The heat that is introduced to the evaporator is transferred to the condenser by the working fluid, which functions

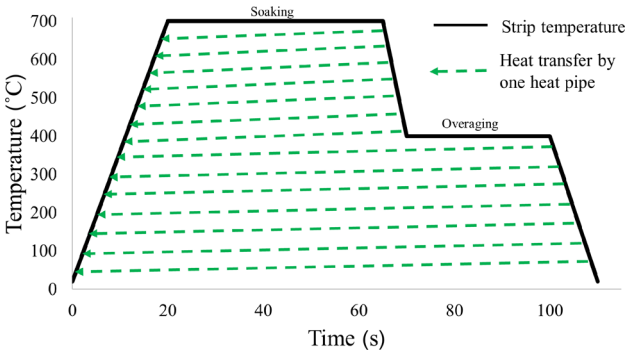

Fig. 1 Typical annealing cycle and linking cooling stage to heating stage

[1]Corresponding author.

Contributed by the Heat Transfer Division of ASME for publication in the Journal of Heat Transfer. Manuscript received August 22, 2018; final manuscript received January 14, 2019; published online July 22, 2019. Assoc. Editor: Luisa Rossetto.

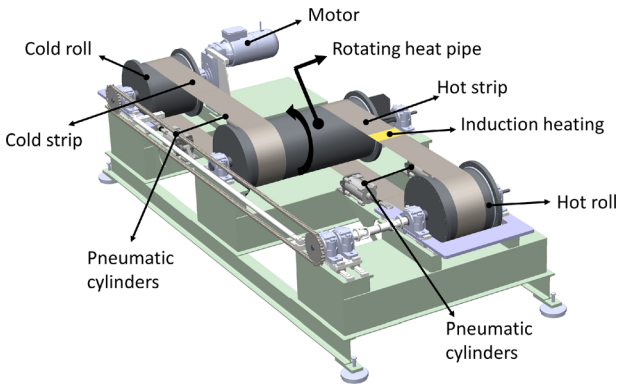

Fig. 2 CAD view of the proof of principle [11] (Reprinted with permission from Elsevier copyright 2018)

as a thermal energy carrier [4]. The subsequent processes occurring in a rotating heat pipe are: (i) heat added to the evaporator causes the liquid to evaporate, (ii) the vapor travels to the condenser passing through the adiabatic section due to the pressure difference induced, (iii) the vapor dissipates its heat in the condenser section condensing back to liquid, (iv) the liquid returns to the evaporator by the centrifugal force and the static pressure head, completing the cycle [3,5].

Rotating heat pipes have been widely investigated for use in various applications. They have been shown to be very effective for cooling of drill tips [6,7]. Similarly, rotating heat pipes have been successfully applied for the cooling of rotating electrical machines [8–10].

Although applications of rotating heat pipes are not limited to the aforementioned literature sources, such applications use heat pipes much smaller in size and in diameter-to-length ratio compared to the rotating heat pipes considered in the current work. In this study, the selected size of the rotating heat pipe is 0.5 m in diameter in order to avoid plastic deformation of tensioned strips and 3 m in length to accommodate the strips. This results in a diameter to length ratio of 0.17.

The concept of transferring heat from a hotter steel strip to a colder one with a rotating heat pipe has been demonstrated using a specially designed experimental setup [11]. This proof of principle setup consists of an exceptionally large cylindrical rotating heat pipe (of 0.5 m in diameter and 1.2 m in length) consisting of two steel strips hemicylindrically wrapped around it. Induction is used to heat one of the strips. The heat pipe uses demineralized water as a working fluid. The strip that is heated by induction is fed to the evaporator section of the heat pipe and cools down as it transfers its heat to the heat pipe. The colder strip is heated up by the heat transferred by the hot strip (Fig. 2). Heat has been successfully transferred from one strip to the other at various strip line speeds up 10 m/s.

In the heat pipe assisted annealing concept, each heat pipe transports some of the total heat from the cooling strip to the heating strip. With a limited number of heat pipes, most of the heat

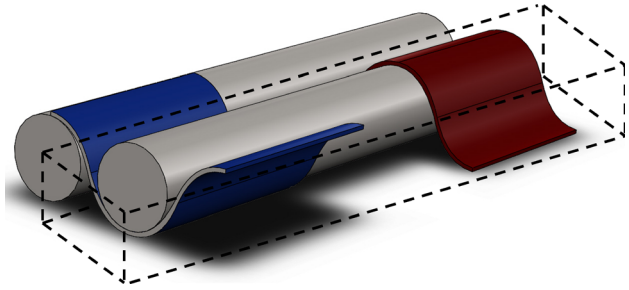

Fig. 4 Building block of the simulation model

can be reused in the process. In order to operate up to 700 °C, different working fluids need to be used for different temperature ranges due to constraints of vapor pressure and long-term fluid stability. Only final heating and cooling of the steel strip is performed in a conventional way. The strip being heated and the strip being cooled may be part of the same strip. In this case, the strip that is heated is reversed after the conventional heating section (Fig. 3) [2].

To study the technical and economic feasibility of the technology, a dynamic simulation of a heat pipe assisted annealing line is developed. This line concept can be seen as a collection of building blocks. Each block comprises of a rotating heat pipe and strip parts wrapped around the heat pipe. The current paper focuses on the building blocks interaction and the overall behavior of the system, rather than on providing a detailed description of underlying physics. Nonetheless, some of the architecture of the building block is provided. With the information gathered from the simulation results, the thermal cycle of the strip and associated energy savings can be computed for different line configurations. This will allow for determining the economic feasibility of the heat pipe assisted annealing line concept.

2 Simulation Model

The heat pipe assisted annealing simulation model comprises of modular components called building blocks. Each building block consists of a rotating heat pipe and two strips wrapped around the heat pipe (Fig. 4). The simulation model essentially represents the interaction between these building blocks. The number of heat pipes in the installation is equal to the number of building blocks inside the simulation model. The building blocks are interlinked by the connecting strips.

The model assumes no heat losses to the outside and no additional rolls apart from the heat pipes. The heat losses are not included to the study because they are strongly dependent on the properties of the plant insulation. The exclusion of the heat losses from the analysis ensures that the focus lies on the energy savings brought by thermally linking the heating and the cooling cycles.

Conventional heating and conventional cooling are calculated based on the amount of heat required to reach the target temperatures. The overaging stage of the annealing cycle is not included in the simulations. This is because overaging does not have an

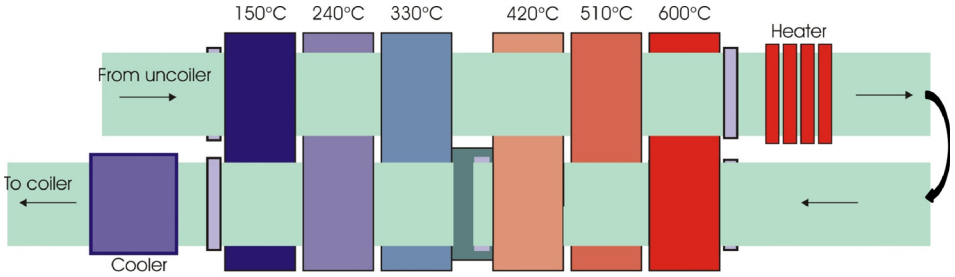

Fig. 3 Heat pipe assisted annealing conceptual representation [2]

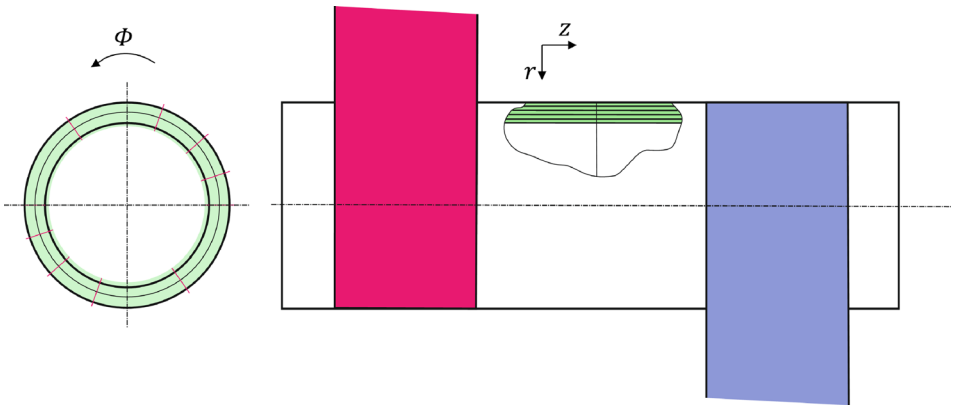

Fig. 5 Building block meshing

effect on the energy saving amount and the location of the overaging stage in a plant strongly depends on the plant layout and the type of the strips to be annealed.

2.1 Building Block. The building block comprises of the meshed heat pipe wall, heat pipe interior, and strips. The wall of the heat pipe is meshed in axial, radial, and angular directions. The strip is meshed only in the angular direction, as the Biot number is lower than 0.1 for the strip thickness.

The hotter strip is in contact with the evaporator and the colder strip is fed to the condenser. The adiabatic section is situated between the evaporator and the condenser. Moreover, there are two more adiabatic sections at the two ends of the heat pipe, which are called dead zones. The angular mesh is slightly finer near the first contact point of the strip with the heat pipe in order to better capture the boundary condition change. The mesh structure is mirrored for the other half circumference. The heat pipe wall is divided into several layers in the radial direction (Fig. 5).

A node of the roll wall is modeled with Eq. (1). The properties are calculated with reference to the average wall temperature for each heat pipe

$$\frac{\partial(\rho_w c_{p_w} T_w)}{\partial t} = \rho_w c_{p_w} u_\Phi \frac{1}{r}\frac{\partial T_w}{\partial \Phi} + \frac{\partial}{\partial z}\left(k_w \frac{\partial T_w}{\partial z}\right) + \frac{1}{r}\frac{\partial}{\partial r}\left(k_w r \frac{\partial T_w}{\partial r}\right) \tag{1}$$

When the above equation is integrated over the control volume, the conductive resistances in the radial and axial directions are found as follows:

$$R_{\text{radial}} = \frac{\ln(r_o/r_i)}{\Delta\Phi\, k_w\, \Delta z} \tag{2}$$

$$R_{\text{axial}} = \frac{\Delta z}{k_w A'} \tag{3}$$

The innermost nodes are subjected to the liquid layer temperature, whereas the outermost nodes below the strip are subjected to the strip temperature. For a strip node, Eq. (4) applies. The strip properties are calculated with reference to the entering strip temperatures

$$\frac{\partial(\rho_s c_{p_s} T_s)}{\partial t} = \rho_s c_{p_s} u_\Phi \frac{1}{r}\frac{\partial T_s}{\partial \Phi} \tag{4}$$

The strip is subjected to the contact heat transfer with the outermost nodes of the heat pipe. The contact resistance between the strip and the heat pipe is defined with the below equation:

$$R_{\text{contact}} = \frac{1}{h_{\text{contact}}\, w_s\, l_{\text{node}}} \tag{5}$$

A previous study carried out in the context of the heat pipe-assisted annealing project describes the contact heat transfer coefficient between a steel strip and a rotating heat pipe [11]. However, the numerical model described in this previous work is not sufficiently fast. Therefore, the contact heat transfer coefficient values in the current work are calculated based on regression analysis of the data generated from the numerical model in Ref. [11]. To carry out a dimensionless analysis, Nusselt number is selected as the dependent variable.

$$\text{Nu} = \frac{h_{\text{contact}}\, D_{\text{roll}}}{k_g} \tag{6}$$

The Nusselt number is calculated for a parametric study of strip thickness, specific tension, roll radius, and gas properties. Using multiple regression analysis, the resulting Nusselt number correlation is found as in the below equation:

$$\text{Nu} = 0.394\, \gamma^{-1}\, \varepsilon^{\left(-\frac{2}{3}\right)} \tag{7}$$

with

$$\varepsilon = \frac{\mu_g\, u_s}{\sigma_s\, \text{th}_s} \tag{8}$$

$$\gamma = 0.084\eta^2 - 0.25\eta + 0.643 \tag{9}$$

$$\eta = \frac{\sigma_s\, \text{th}_s}{p_a\left(\dfrac{D_{\text{roll}}}{2}\right)} \tag{10}$$

The exterior gas properties are calculated based on a typical protective gas composition used commonly in the annealing of steel (5% H_2/95% N_2) [12]. It should be noted that the thermal conductivity and the viscosity of the interstitial gas are temperature dependent and this dependency is accounted for in the model.

The specific tension applied to the strip at room temperature is taken as 30 MPa. At higher temperatures, a reduction factor describing the change of actual yield strength with respect to the yield strength at room temperature as a function of temperature is applied [13].

The interior dynamics of the rotating heat pipe is described with a model derived from a previous work performed in the context of the same project [14]. The two main components of the model are the liquid and the vapor, which are modeled as lumped masses. Each phase is axially meshed (Fig. 6). Each node is a lump mass characterized by a unique thermodynamic state. The mesh is staggered such that the temperatures and pressures are located at cell centers, whereas velocities are located at cell faces.

The model description includes the equations for mass, momentum, and energy. The radial and the angular distributions of the

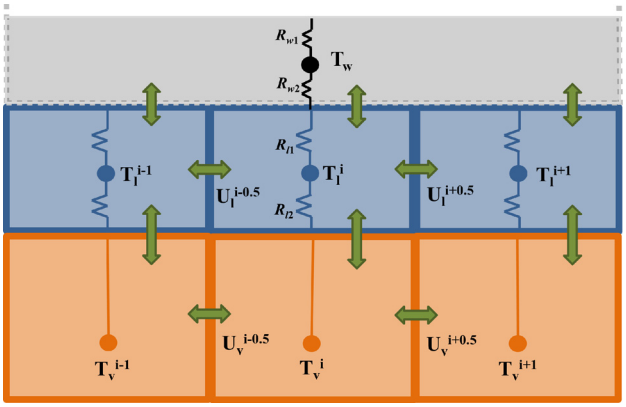

Fig. 6 Heat pipe interior meshing

axial velocity are not accounted for. The generic mass equation for a given liquid or vapor node is shown in the below equation:

$$\frac{\partial(\rho\,\mathrm{d}V)}{\partial t} = \frac{1}{r}\frac{\partial(\rho r u_r\,\mathrm{d}V)}{\partial r} + \frac{\partial(\rho u_z\,\mathrm{d}V)}{\partial z} \tag{11}$$

The phase change rate is described with the below equation:

$$\dot{m}_{\mathrm{ph}} = \frac{T_l - T_v}{R_{v-l}\,H_{fg}} \tag{12}$$

where R_{v-l} is the radial thermal resistance between the vapor node and the liquid node. It can be defined as follows:

$$R_{v-l} = R_{l2} + R_{\mathrm{ph}} = \left[\frac{\ln\left(\dfrac{\frac{D_i}{2} - \frac{\mathrm{th}_l}{2}}{\frac{D_i}{2} - \mathrm{th}_l}\right)}{k_l\,(2\pi - \theta)\,\Delta z} + R_{\mathrm{ph}}\right] \tag{13}$$

where R_{ph} is the phase change thermal resistance which is neglected in the presented work [15]. The liquid thermal resistance R_{l2} is defined in Fig. 6.

The convective terms in the liquid momentum equation are assumed to be negligible [16–18]. The generic momentum equation is described with Eq. (13), where the term in brackets is valid only for the vapor phase. A central difference scheme is used during the calculation of the convective term. The viscous term is approximated with a friction factor [15,19,20].

$$\frac{\partial(\rho u_z)}{\partial t} + \left[\frac{\partial(\rho u_z u_z)}{\partial z}\right] = -\frac{\partial p}{\partial z} + \frac{\rho f u_z |u_z|}{2D_h} \tag{14}$$

The pressure difference in the axial direction for vapor is related to the vapor pressure difference. For the liquid, it is related to the static liquid head and the centrifugal force [18]. For laminar flow where Re is lower than 2100, the friction factor (f) is taken as $64/\mathrm{Re}$. For turbulent flow, the friction factor is calculated as $0.0791/\mathrm{Re}^{0.25}$ [15,19,20].

The energy equation for liquid is defined as follows:

$$\frac{\partial(\rho c_p T\,\mathrm{d}V)}{\partial t} + \frac{\partial(\rho c_p u_z T\,\mathrm{d}V)}{\partial z} + \frac{\partial(\rho c_p u_r T\,\mathrm{d}V)}{\partial r} = -\frac{\partial \dot{q}_r}{\partial r}\,dr \tag{15}$$

Assuming that the heat transfer in the radial direction and phase change are dominant over the heat transfer in the axial direction [16–18], the energy equation for a liquid node is written as follows:

$$\rho V\frac{d(c_p T_l)}{dt} = \frac{T_w - T_l}{R_{w-l}} + \frac{T_v - T_l}{R_{v-l}} \tag{16}$$

where R_{w-l} is the radial thermal resistance between the wall node and the liquid node. It is defined as follows:

$$R_{w-l} = R_{w2} + R_{l1} = \left[\frac{\ln\left(\dfrac{\frac{D_i}{2} + \frac{\mathrm{th}_w}{2}}{\frac{D_i}{2}}\right)}{k_w\,2\pi\,\Delta z} + \frac{\ln\left(\dfrac{\frac{D_i}{2}}{\frac{D_i}{2} - \frac{\mathrm{th}_l}{2}}\right)}{k_l\,(2\pi - \theta)\,\Delta z}\right] \tag{17}$$

where the thermal resistances R_{w2} and R_{l1} are defined in Fig. 6.

Due to the axisymmetric geometry, the thermal resistance caused by the liquid pool is distributed across the interior circumference. In order to determine the flow pattern, the dimensionless Froude number is calculated and then compared to the critical Froude number for complete annular flow in a finite cylinder [21]

$$\mathrm{Fr} = \frac{\omega^2\left(\frac{D}{2}\right)}{g} \tag{18}$$

$$\mathrm{Fr}_c = 20.03\,(1-\chi)^{-2.421} \tag{19}$$

In the case of a liquid pool forming, the heat transfer is assumed to take place only through the thin liquid film that is pulled by rotation. The average thickness of the thin liquid film is calculated with Eq. (20), whereas the angle of the liquid pool is calculated using the below equation [22]:

$$\bar{\delta} = \frac{5}{6}\frac{\left(\frac{D_i}{2}\right)}{\sqrt{\frac{\rho\,g\,D_i}{2\,\mu\,\omega}}} \tag{20}$$

$$\chi = \frac{1}{2\pi}(\theta - \sin\theta) \tag{21}$$

The liquid resistance within the condenser and adiabatic sections are associated with thermal conduction only [23,24]

$$R_l = \frac{\ln\left(\dfrac{\frac{D_i}{2}}{\frac{D_i}{2} - \mathrm{th}_l}\right)}{(2\pi - \theta)k_l\,\Delta z} \tag{22}$$

The liquid resistance at the evaporator side is described as a mixed convection evaporator model [17,25,26], where natural convection is taken to be dominant in the liquid. It is calculated as follows [17]:

$$R_{l,e} = \frac{\ln\left(\dfrac{\frac{D_i}{2}}{\frac{D_i}{2} - \mathrm{th}_l}\right)}{(2\pi - \theta)\,\mathrm{Nu}_m\,k_l\,\Delta z} \tag{23}$$

where Nu_m is defined as

$$(\mathrm{Nu}_m)^{7/2} = (\mathrm{Nu}_f)^{7/2} + (\mathrm{Nu}_n)^{7/2} \tag{24}$$

where Nu_f is taken as 1 due to relatively low Reynolds number liquid flow and Nu_n is defined as:

$$\mathrm{Nu}_n = 0.133\,\mathrm{Ra}^{0.375} \tag{25}$$

The Rayleigh number (Ra) for a rotating heat pipe is calculated with the below equation [16]:

$$\mathrm{Ra} = \frac{\beta\rho_l\left(\frac{D}{2}\omega^2\right)\Delta T\delta^3}{\mu_l\alpha_l} \tag{26}$$

Natural convection is present when the calculated Rayleigh number exceeds the value of 400. Below this value, natural convection does not play a role as the prevailing heat transfer mechanism is conduction [26].[2]

As the dynamics of the vapor is much faster compared to the dynamics of other components, the vapor energy equation is solved with an algebraic balance equation, rather than a differential equation[3]

$$\frac{p_v}{T_v} = \frac{\rho_v \mathcal{R}_g}{M} \tag{27}$$

Where the vapor is assumed to be saturated everywhere and its pressure is calculated with the Antoine equation:

$$p_v = 10^{A-\frac{B}{T_v+C}} \tag{28}$$

The fluid properties are calculated based on the average temperature of the corresponding phase for the given time-step [27–31].

2.2 System Solver. The governing equations describing a building block consist of both first-order ordinary differential equations and algebraic equations. The equations are formulated in their discretized forms in space. Given an initial condition and boundary conditions, the set of equations can be solved with an integration method.

The entering strip temperature to the evaporator and the condenser of a certain heat pipe is equal to the exiting strip temperature of the preceding building block. The boundary condition applied to the outer surface of the strips and the outer surface of the heat pipe wall not in contact with the strips is:

$$r = r_o \Rightarrow -k\frac{dT}{dr} = 0 \tag{29}$$

At the two ends of the heat pipe, following conditions apply:

$$z = 0 \wedge z = L \Rightarrow u_l = u_v = 0 \wedge \frac{dT}{dz} = 0 \tag{30}$$

The boundary condition at the symmetry line of the heat pipe is:

$$r = 0 \Rightarrow \frac{dT}{dr} = 0 \tag{31}$$

The initial conditions for each heat pipe are selected such that the heat pipe starts with a uniform temperature throughout and at an idle state. The initial temperatures for the heat pipes increase from the first heat pipe to the last, with an interval of 7 °C between cesium heat pipes and with an interval of 4 °C between the rest of the heat pipes.

Each building block is solved for a finite time-step. After the effects of the time-step have been calculated for all the building blocks, the resulting strip temperatures entering the building blocks as well as the material properties of each heat pipe are updated. The time-step is selected as the time it takes for a strip element to travel over the heat pipe. It is defined with the following equation:

$$\Delta t = \frac{\frac{\pi D_o}{2}}{u_s} \tag{32}$$

The problem at hand is stiff. Therefore, the system of equations is solved implicitly with the "MATLAB ode15i" function.

The number of nodes for one building block is in total 280. The heat pipe interior is composed of 20 nodes, the heat pipe wall is composed of $5 \times 5 \times 10$ nodes in the radial, axial and angular directions, respectively. The strips are composed of five nodes each in the angular direction.

3 Simulation Results

3.1 Annealing Line Configurations. In a typical continuous annealing line, the strip enters the line at room temperature. It is then heated up to the target temperature of 700 °C. The line speed in the continuous annealing is around 10 m/s. In the light of this information, the simulations are run for a number of configurations with heat pipes numbering between 50 and 100.

The selection of the working fluids is critical for this concept. It determines the temperatures at which the heat pipes can operate, has a major influence on their performance and together with the shell material it restricts lifetime. The working fluids are selected based on their vapor pressures at the relevant temperature range as well as their performance, stability, and compatibility with stainless steel, safety aspects, and availability. Accordingly, the working fluids are determined as water, Dowtherm A, phenanthrene and cesium to cover the temperature range up to 700 °C. The vapor pressures of these fluids are provided in Fig. 7. Special attention should be paid to the organics, which can decompose to produce noncondensable gas outside their intended temperature range.

The fill ratio is selected such that the critical Froude number calculated with Eq. (19) yields a higher value than the actual Froude number obtained through Eq. (18). This ensures a flow pattern where a complete annular flow is not formed.

The heat pipe diameter and length are 0.5 m and 3 m, respectively. The thickness of the strip varies between 0.15 mm and 0.30 mm, whereas its width is kept fixed at 1 m. The line speed varies from 8 to 10 m/s.

3.2 Near Steady-State Results. Three cases are selected as representative results of near steady-state conditions. Installation properties and process parameters for these cases are shown in Table 1. For each case, the energy saving of the system is calculated as follows:

$$\frac{H_s^{\mathrm{exit}} - H_s^{20\,^\circ\mathrm{C}}}{H_s^{700\,^\circ\mathrm{C}} - H_s^{20\,^\circ\mathrm{C}}} \tag{33}$$

where H_s^{exit} is the enthalpy of the exiting strip from the condenser of the last heat pipe, $H_s^{20\,^\circ\mathrm{C}}$ is the enthalpy of the entering strip and $H_s^{700\,^\circ\mathrm{C}}$ is the enthalpy of the strip at the target temperature.

Figure 8 shows the strip temperature evolution for case 1. Strip temperature changes over different heat pipes can be clearly seen when the heat pipe number in the x-axis is followed. The straight lines in the figure correspond to conventional heating/cooling and thermal soaking stages.

In this figure, it is seen that each heat pipe contributes to the strip heating and cooling. The close-up of part of the heating cycle in Fig. 8 shows that the magnitude of these contributions may differ between various heat pipes. It is seen that the heat transfer via cesium heat pipes is significantly more effective compared to the heat transfer achieved via heat pipes filled with organic fluids

[2]In all simulations, the Rayleigh number is larger than 400 for the water, Dowtherm A, and phenanthrene heat pipes. For the cesium heat pipes, the Rayleigh number is below 1 at all times, resulting in the absence of natural convection at the evaporator.

[3]It should be noted that the ideal gas law is not a good approximation for Dowtherm A and phenanthrene when the pressure is above 10 bar. In such cases, the compressibility factor should be taken into account. In the current application, the pressure of the heat pipes containing Dowtherm A and phenanthrene always remains below 5 bar.

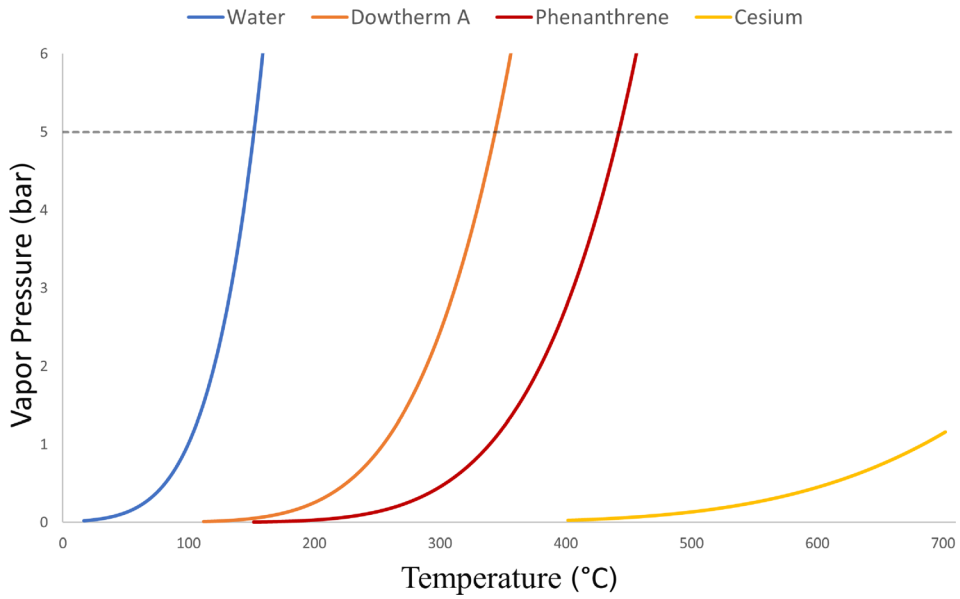

Fig. 7 Vapor pressure of working fluids

Table 1 Representative simulated cases

Parameter	Unit	Case 1	Case 2	Case 3
Total no. of heat pipes (HP)	—	70	50	100
Water HP #		10	0	20
Dowtherm A HP #		20	20	25
Phenanthrene HP #		20	20	25
Cesium HP #		20	10	30
Line speed	(m/s)	8	10	8
Strip thickness	(mm)	0.20	0.15	0.30
Fill ratio	(%)	∼32	∼32	∼32

(Dowtherm A and phenanthrene). The main reason for such difference in the effectiveness of working fluids is the different thermal conductivity of the liquids. The typical overall thermal resistance of a cesium heat pipe is ∼0.001 K/W, whereas it varies between 0.006 and 0.007 K/W for heat pipes filled with organic fluids. For water heat pipes, this value is ∼0.0025 K/W.

Still, heat pipes filled with organic fluids are indispensable to the concept in order to cover the intermediate temperature range. A too low temperature, and thus pressure of a cesium heat pipe, is likely to result in high vapor velocities, eventually encountering sonic limitations [32,33].

Consequently, the heat transfer rate via heat pipes is calculated as ∼4.5 MW for case 1. This corresponds to an energy saving of 75%.

Figures 9 and 10 show the strip temperature evolution patterns for cases 2 and 3, which are obtained by the variation of the properties shown in Table 1.

In case 2, the smaller number of heat pipes as well as the larger line speed results in a relatively lower energy saving of 62%, although the strip thickness is lower compared to case 1. This is also caused by the higher ratio of the number of heat pipes filled with organic fluid to the total number of heat pipes. The calculated heat transfer rate via heat pipes is ∼3.5 MW for this case.

In case 3, the strip thickness and the number of heat pipes are doubled in comparison to case 2. The line speed is selected as 8 m/s due to the thicker strip. With a total heat transfer rate of ∼6.8 MW via 100 heat pipes, the resulting energy saving is found to be 75% for case 3. For this case, the typical heat transfer rate for individual heat pipes are 86 kW, 32 kW, 35 kW, and 112 kW for water, Dowtherm A, phenanthrene, and cesium heat pipes, respectively.

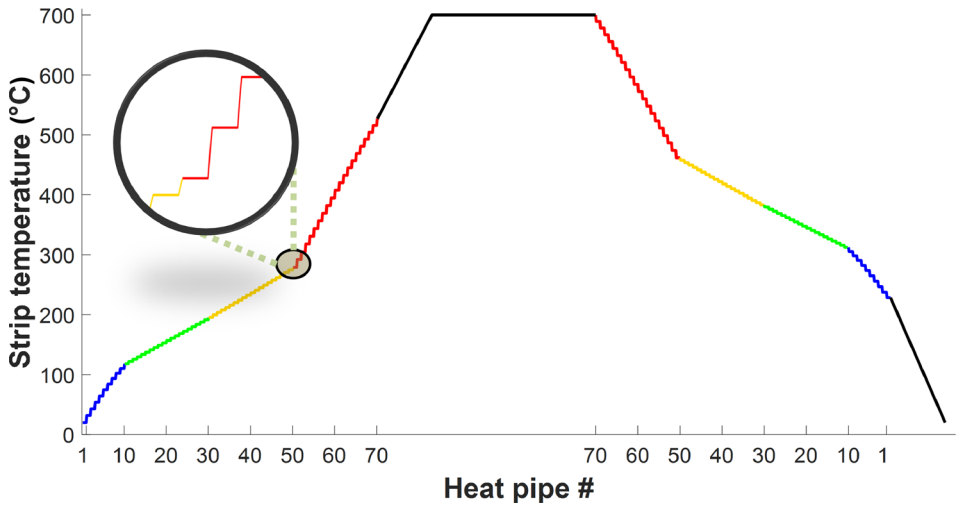

Fig. 8 Simulation case 1: near steady-state

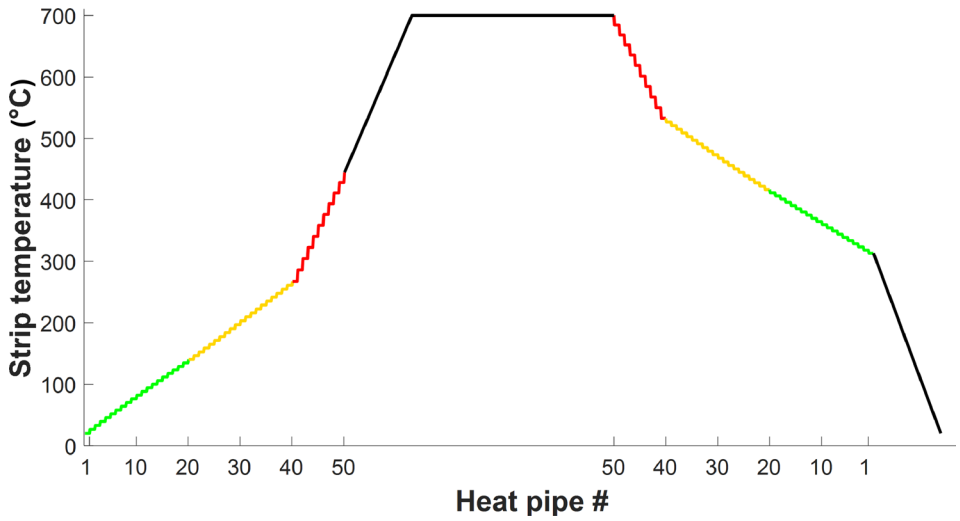

Fig. 9 Simulation case 2: near steady-state

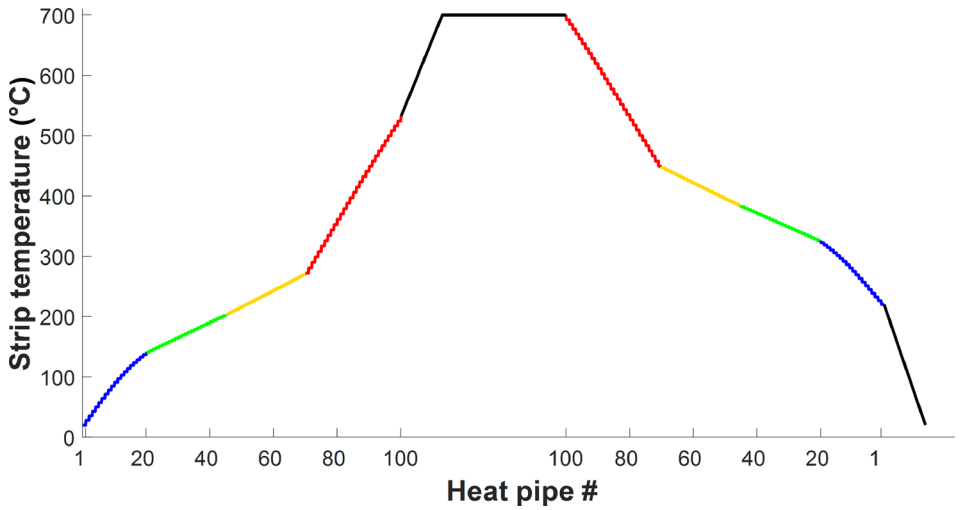

Fig. 10 Simulation case 3: near steady-state

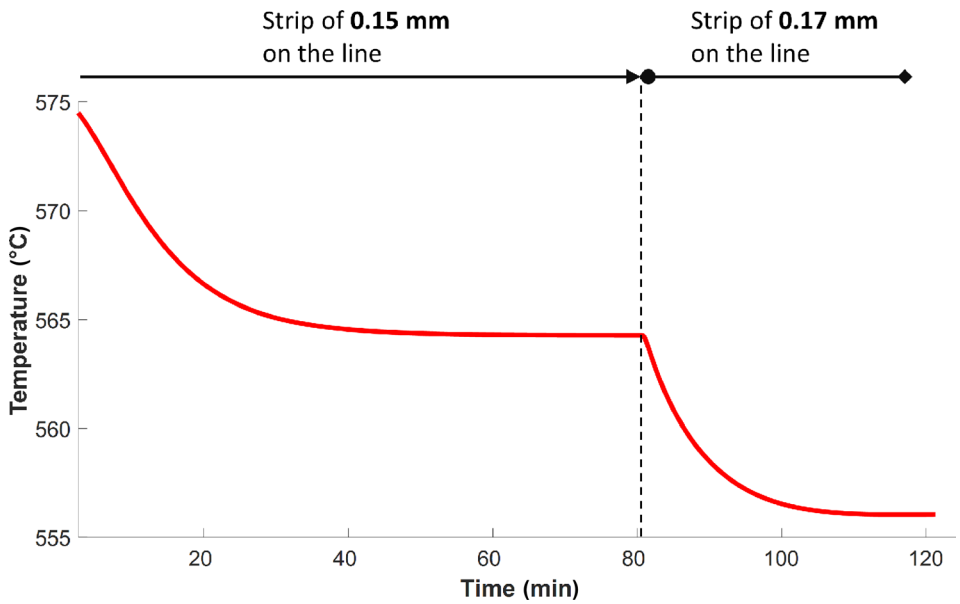

Fig. 11 Dynamics of a cesium heat pipe at a strip thickness change

The average head necessary to bring the liquid from the condenser to the evaporator is ~2.5 μm for water heat pipes, whereas it varies 4–5 μm for Dowtherm A and phenanthrene heat pipes. This demonstrates the superior properties of water [23] especially due to its very high specific latent heat. Cesium also has superior properties compared to the organics (higher specific latent heat and liquid density). However, the required liquid head is comparable to the organic heat pipes because more heat is transferred through a cesium heat pipe compared to the heat transferred through an organic heat pipe.

For all of these cases, it is clearly seen that the thermal cycle requirements of annealing can be met with the benefit of substantial energy saving.

3.3 Transient Results. With the model, detailed state information, such as temperature, pressure, liquid height, and vapor velocity in a heat pipe, is obtained. In addition, the time-based calculation method allows for time tracking of such parameters.

In Fig. 11, the temperature of the last cesium heat pipe following a transition to a thicker strip is shown. It is seen that the temperature of the heat pipe decreases and reaches a new near steady-state.

The reason for the decrease in the heat pipe interior temperature can be explained by considering the system as a whole. Looking at the last heat pipe in the line, the entering strip temperature to the evaporator is always equal to the soaking temperature, in this case to 700 °C. However, the entering strip temperature to the condenser decreases after the strip thickness increases. This is because the increased thickness of the strip has a higher thermal inertia compared to the thinner strip. This results in a lower strip temperature increase during the heating stage and translates into a higher heat output from the heat pipe after the strip thickness change.

It is important to note that the thermal cycle requirements are met at all times during the transition between these near steady-states.

4 Conclusions

In this paper, the dynamic modeling of the heat pipe assisted annealing line is described. The model is composed of a series of building blocks, each of them representing one rotating heat pipe and steel strips hemicylindrically wrapped around it. The described model is used as a process model to simulate the behavior of the system. Additionally, it is used as an engineering support model to optimize the installation configuration with respect to the number of heat pipes and the capacity of the conventional heater.

The simulation results show that the thermal cycle requirements can be satisfied with this new technology. A change in strip dimensions during operation does not compromise the performance of the line. The efficiency of the liquid metal heat pipes is much higher compared to the organic heat pipes. However, the organic heat pipes are indispensable to the concept as they are instrumental in covering the intermediate temperature range during annealing. With this concept, an energy saving of 70% remains feasible with the heat pipe number varying between 50 and 100.

Next steps for the simulation of this technology include the optimization of the plant layout including overaging followed by a sensitivity and economic analysis. It is also important to investigate the effects of noncondensable gas and the performance of each working fluid, which are critical for the high energy saving values and the technical feasibility of the concept.

Acknowledgment

This work is part of a collaboration project named "Heat Pipe Assisted Annealing" between Tata Steel, TU Delft and Drever International. The assistance of the collaborating project members is gratefully acknowledged.

Nomenclature

A' = cross-sectional area, m^2
A, B, C = Antoine equation constants
c_p = specific heat, J/(kg K)
D = diameter, m
D_h = hydraulic diameter, m
f = friction factor
Fr = Froude number $(\omega^2(D/2))/g$
g = gravitational acceleration, m/s^2
h = heat transfer coefficient, $W/(m^2 K)$
H = enthalpy, J/kg
H_{fg} = latent heat, J/kg
k = thermal conductivity, W/(m K)
l = length, m
L = heat pipe length, m
m = mass flow rate, kg/s
M = molecular weight, g/mol
Nu = Nusselt number, hD/k
p = pressure, Pa
$\dot{q}$ = heat flow, W
r = radial coordinate
R = thermal resistance, K/W
R_g = universal gas constant, m^3 Pa/K mol
Ra = Rayleigh number $(\beta\rho_l((D/2)\omega^2)\Delta T\delta^3)/\mu_l\alpha_l$
Re = Reynolds number, $\rho u D/\mu$
t = time, s
T = temperature, K
th = thickness, m
u = velocity, m/s
V = volume, m^3
w = width, m
z = axial coordinate

Greek Symbols

α = thermal diffusivity, m^2/s
β = thermal expansion coefficient, K^{-1}
γ = compressibility factor
δ = liquid layer thickness, m
$\bar{\delta}$ = average liquid layer thickness, m
Δt = time step, s
ΔT = temperature difference, K
Δz = axial distance difference, m
$\Delta\Phi$ = angular difference, rad
ε = foil bearing number $(\mu_g u_s)/(\sigma_s \mathrm{th}_s)$
η = pressure ratio $((\sigma_s \mathrm{th}_s)/(p_a(D_{\mathrm{roll}}/2)))$
θ = angle of the liquid pool, rad
μ = dynamic viscosity, Pa·s
ρ = density, kg/m^3
σ = tension, Pa
Φ = angular coordinate
χ = fill ratio
ω = rotational speed, rad/s

Subscripts

a = ambient
c = critical
e = evaporator
f = forced convection
g = interstitial gas
i = inner
l = liquid
m = mixed convection
n = natural convection
o = outer

ph = phase change
r = radial
s = strip
v = vapor
w = wall
z = axial
Φ = angular

References

[1] ASM International Handbook Committee, 1991, *ASM Handbook* (Heat Treating, Vol. 4), American Society for Metals, Materials Park, OH, pp. 42–55.
[2] Paulussen, G., 2011, "Heat Pipe Assisted Strip Treatment," Patent No. WO 2011012257 A1.
[3] Gray, V. H., 1969, "The Rotating Heat Pipe—A Wickless Hollow Shaft for Transferring High Heat Fluxes," ASME Paper No. 69-HT-19.
[4] Zuo, Z. J., and Faghri, A., 1998, "A Network Thermodynamic Analysis of the Heat Pipe," Int. J. Heat Mass Transfer, **41**(11), pp. 1473–1484.
[5] Ballback, L. J., 1969, "The Operation of a Rotating, Wickless Heat Pipe," Ph.D. thesis, Naval Postgraduate School, Monterey, CA.
[6] Jen, T. C., Chen, Y. M., and Gutierrez, G., 2003, "Thermal Performance of Heat Pipe Drill: Experimental Study," ASME Paper No. HT2003-47096.
[7] Jen, T. C., Gutierrez, G., Eapen, S., Barber, G., Zhao, H., Szuba, P. S., Labataille, J., and Manjunathaiah, J., 2002, "Investigation of Heat Pipe Cooling in Drilling Applications—Part I: Preliminary Numerical Analysis and Verification," Int. J. Mach. Tools Manuf., **42**(5), pp. 643–652.
[8] Ponnappan, R., He, Q., and Leland, J., 1997, "Test Results of a High Speed Rotating Heat Pipe," 32nd Thermophysics Conference, Atlanta, GA, June 23–25, p. 2543.
[9] Kukharskii, M. P., 1974, "Closed Evaporative Cooling of Rotating Electrical Machines," J. Eng. Phys., **27**(3), pp. 1090–1096.
[10] Groll, M., Krahling, H., and Munzel, W. D., 1978, "Heat Pipes for Cooling of an Electric Motor," J. Energy, **2**(6), pp. 363–367.
[11] Celik, M., Devendran, K., Paulussen, G., Pronk, P., Frinking, F., de Jong, W., and Boersma, B. J., 2018, "Experimental and Numerical Investigation of Contact Heat Transfer Between a Rotating Heat Pipe and a Steel Strip," Int. J. Heat Mass Transfer, **122**, pp. 529–538.
[12] Chandler, H., 1994, *Heat Treater's Guide: Practices and Procedures for Irons and Steels*, American Society for Metals, Materials Park, OH, p. 8.
[13] Union, C. E., 2005, "Eurocode 3: Design of Steel Structures—Part 1–2: General Rules – Structural Fire Design," The European Union Per Regulation, Brussels, Belgium, Report No. EN 1993-1-2:2005: E, pp. 22–23.
[14] Celik, M., Paulussen, G., van Erp, D., de Jong, W., and Boersma, B. J., 2018, "Transient Modelling of Rotating and Stationary Cylindrical Heat Pipes: An Engineering Model," Energies, **11**(12), p. 3458.
[15] Reay, D., McGlen, R., and Kew, P., 2013, *Heat Pipes: Theory, Design and Applications*, Butterworth-Heinemann, Waltham, MA, pp. 20–22.
[16] Bertossi, R., Guilhem, N., Ayel, V., Romestant, C., and Bertin, Y., 2012, "Modeling of Heat and Mass Transfer in the Liquid Film of Rotating Heat Pipes," Int. J. Therm. Sci., **52**, pp. 40–49.
[17] Song, F., Ewing, D., and Ching, C. Y., 2003, "Fluid Flow and Heat Transfer Model for High-Speed Rotating Heat Pipes," Int. J. Heat Mass Transfer, **46**(23), pp. 4393–4401.
[18] Harley, C., and Faghri, A., 1995, "Two-Dimensional Rotating Heat Pipe Analysis," ASME J. Heat Transfer, **117**(1), pp. 202–208.
[19] Ferrandi, C., Iorizzo, F., Mameli, M., Zinna, S., and Marengo, M., 2013, "Lumped Parameter Model of Sintered Heat Pipe: Transient Numerical Analysis and Validation," Appl. Therm. Eng., **50**(1), pp. 1280–1290.
[20] Cao, Y., and Faghri, A., 1991, "Transient Multidimensional Analysis of Nonconventional Heat Pipes With Uniform and Nonuniform Heat Distributions," ASME J. Heat Transfer, **113**(4), pp. 995–1002.
[21] Baker, J., Oliver, T., Lin, L., Ponnapan, R., and Leland, J., 2001, "Correlations of Critical Froude Number for Annular-Rimming Flow in Rotating Heat Pipes," ASME J. Fluids Eng., **123**(4), pp. 909–913.
[22] Lin, L., and Faghri, A., 1997, "Heat Transfer Analysis of Stratified Flow in Rotating Heat Pipes With Cylindrical and Stepped Walls," Int. J. Heat Mass Transfer, **40**(18), pp. 4393–4404.
[23] Daniels, T. C., and Al-Jumaily, F. K., 1975, "Investigations of the Factors Affecting the Performance of a Rotating Heat Pipe," Int. J. Heat Mass Transfer, **18**(7–8), pp. 961–973.
[24] Li, H. M., Liu, C. Y., and Damodaran, M., 1993, "Analytical Study of the Flow and Heat Transfer in a Rotating Heat Pipe," Heat Recovery Syst. CHP, **13**(2), pp. 115–122.
[25] Song, F., Ewing, D., and Ching, C. Y., 2004, "Experimental Investigation on the Heat Transfer Characteristics of Axial Rotating Heat Pipes," Int. J. Heat Mass Transfer, **47**(22), pp. 4721–4731.
[26] Song, F., Ewing, D., and Ching, C. Y., 2008, "Heat Transfer in the Evaporator Section of Moderate-Speed Rotating Heat Pipes," Int. J. Heat Mass Transfer, **51**(7–8), pp. 1542–1550.
[27] Yaws, C. L., 1999, *Chemical Properties Handbook: Physical, Thermodynamics, Environmental Transport, Safety, and Health Related Properties for Organic and Inorganic Chemicals*, McGraw-Hill, New York.
[28] Dow Chemical Company, 1997, "Dowtherm, A. Heat Transfer Fluid—Product Technical Data," Dow Chemical Company, Midland, MI, accessed Aug. 20, 2018, http://msdssearch.dow.com/PublishedLiteratureDOWCOM/dh_0030/0901b803800303cd.pdf
[29] Linstrom, P. J., and Mallard, W. G., 2001, "The NIST Chemistry WebBook: A Chemical Data Resource on the Internet," J. Chem. Eng. Data, **46**(5), pp. 1059–1063.
[30] Ghatee, M. H., and Sanchooli, M., 2003, "Viscosity and Thermal Conductivity of Cesium Vapor at High Temperatures," Fluid Phase Equilib., **214**(2), pp. 197–209.
[31] Colonna, P., and Van der Stelt, T. P., 2004, "FluidProp: A Program for the Estimation of Thermo-Physical Properties of Fluids, Energy Technology Section," Delft University of Technology, Delft, The Netherlands.
[32] Busse, C. A., 1973, "Theory of the Ultimate Heat Transfer Limit of Cylindrical Heat Pipes," Int. J. Heat Mass Transfer, **16**(1), pp. 169–186.
[33] Nemec, P., Čaja, A., and Malcho, M., 2013, "Mathematical Model for Heat Transfer Limitations of Heat Pipe," Math. Comput. Modell., **57**(1–2), pp. 126–136.